CHAPTER 4

Performance Characteristics of a New Curved Double-pass Counter Flow Solar Air Heater

In this chapter, a novel design of counter flow curved double-pass solar air heater (DPSAH) is proposed, and its performance characteristics are numerically investigated and compared with various parallel designs under different flow and geometric conditions. The developed model is first experimentally validated. The hydraulic and thermal performance of various DPSAH designs (smooth curved single pass, smooth parallel curved double-pass, smooth counter curved double-pass, roughened parallel curved double-pass, and roughened counter curved double-pass) show that counter flow curved DPSAH with asymmetrically placed turbulators is thermally better compared to other designs. A maximum of 23% augmentation in thermal performance was observed. To predict the performance of the best design, new correlations for Nusselt number(Nu) and friction factor $\left(f\right)$ are developed in terms of Reynolds number (Re) and relative roughness height (d/H). The data estimated from these correlations are in good agreement with the values of f and Nu predicted from the model.

4.1 Introduction

Since non-renewable energy sources such as coal, petroleum, etc., are depleting fast, the human race reliance on non-conventional energy sources such as solar energy, tidal energy, wind, etc., would be more in demand the coming times. On the one hand, non-renewable based devices or equipment have high efficiency since energy is available in concentrated form. On the other hand, renewable-based appliances, such as solar air heaters (SAH), have low conversion efficiency as energy is available in the diffused form. However, two crucial features of solar-based

energy make it the right choice for future development. One, it is clean and hence environmentally friendly, and second, it is available in abundance. Quantum of solar energy availability can be gauged from the fact that 30 days of sunlight fall on the Earth have the energy equal to the total of all the planet's fossil fuels, both used and unused[136].Thus, the sun's energy would power most of the devices in the future. Hence, new designs must be proposed and investigated for efficiency improvement. Solar air heaters are versatile devices used for crop drying, space heating, desalination, and many other heating applications[2, 41].Its low cost and less maintenance make it preferable over liquid-based solar energy devices as corrosions or freezing are absent.

Though the performance of SAH devices depends on multiple factors such as climatic parameters (solar intensity, wind velocity, and ambient temperature), flow parameters (natural or forced convection), materials (wood, steel plate, insulating materials, glass materials, etc.[17, 83, 89]) and design (flow passage design: single pass or double pass[62, 88], parallel or counter flow [45], inlet design[121]collector passage design: concave or convex[124]).Among all the factors discussed above, design plays a significant role in SAH performance.Solar air heaters are classified as single-pass and multi-pass (parallel [27], counter[67] and recycle [25]).In a single-pass solar air heater (SPSAH), fluid flows in a single channel, i.e., (between absorber surface and transparent glass or between the absorber and insulating wall). In contrast, double pass solar air (DPSAH) heater fluid flows in two channels (between absorber and glass, i.e., upper channel and between the absorber and insulating wall, i.e., lower channel). Based on the previous studies, DPSAH has more thermal performance than SPSAH due to increase in the double heat transfer area, minimising the top loss and increasing fluid interaction time [97, 142].Based on the airflow arrangement, DPSAH is two types (1) Parallel DPSAH (2) counter DPSAH. In parallel DPSAH, air passes in an upper and lower channel in the same orientation; however, in counter DPSAH, air passes the upper and lower channel in opposite directions.

This chapter deals with the investigation of counter flow curved DPSAH with asymmetrically placed ribs on the absorber plate (see Fig.4.1). Flow and thermal behavior of parallel flow in curved DPSAH has already been reported[74]. Some of the relevant literatures are discussed here to bring about the novelty of this work. Recently Mahboub et al.[87]proposed a new design of curved SAH, which had high thermal performance over conventional SAH.Due to the curved nature of the channel, centrifugal forces pushes the mean flow velocity near the absorber wall and consequently enhanced the heat transfer rate.Singh and Singh [124] reported that natural conventional SAH was 43% and 31% lower thermal performance than smooth natural convex and concave design of SAH, respectively.Singh and Singh [123] conducted a numerical analysis of the different types of SAHs, i.e., CPSP (curve plate smooth single pass), FPSP (flat plate smooth single pass), CPDP (curve plate smooth double pass), FPDP (flat plate smooth double pass). It was seen that the thermal efficiency of SAHs in descending order was CPDP > CPSP > FPDP > FPSP. A curved design SAH with different turbulators such as half triangular, quarter-circle, and trapezoidal has been examined computationally by Singh et al. [122]. It was reported that a good

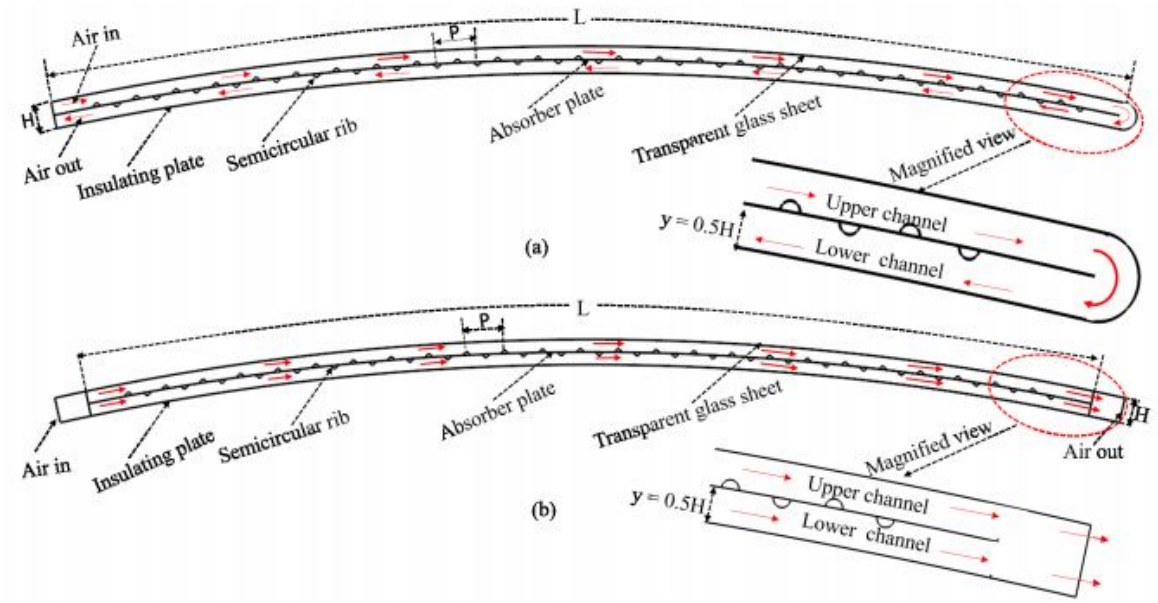

Figure 4.1: A schematic of 2D numerical domain of (a) roughened counter curved DPSAH and (b) roughened parallel curved DPSAH.

balance between thermal and hydraulic performance offered in curved SAH with quarter-circle turbulator. In the previous study by our group[74], it has been observed that a curve parallel DPSAH with asymmetric semicircular rib is thermally more efficient as compared to a curve parallel DPSAH with symmetric circular rib.

Hernandez and Quinonez [45] reported that the thermal performance of flat double-pass counter flow SAH was superior as compared to flat double-parallel flow SAH and single-pass SAH. Yousef and Adam[150] performed a theoretical analysis of single and double pass SAH with porous and without porous material. They found that dual-pass SAH shows 10-12% more thermal efficiency than single-pass at the same operating conditions. Dhiman et al. [12] reported that a parallel flow pack bed SAH shows 11-17% lower thermal efficiency than a counter flow pack bed SAH. The effect of arrangement (staggered and aligned) of turbulators (Aluminum cans) on the thermal performance of DPSAH were studied experimentally by Abdullah et al. [2]. They found that Nusselt number of DPSAH with staggered and aligned designs show 38% and 30%, respectively, more than flat plate DPSAH. Experimental study of the thermal performance of DPSAH with tubular absorber and flat absorber was investigated by Abo-Elfadl et al. [3]. They observed that the average exergy efficiency of tubular absorber was 59% more than flat absorber at 0.025 kg/s. Hassan et al. [43] conducted an experimental analysis of DPSAH having V-corrugated absorber and corrugated perforated absorber for 1/3 air flow through upper channel inlet (DP) and 2/3 air flow through upper channel inlet (DP). It was found that the maximum daily efficiency of V-corrugated designs and perforated absorber was 70.58% and 71.85%, respectively, at 2/3 DP condition. Some other relevant literature on DPSAH has been listed in

Table 4.1 with their main findings. The literatures discussed above reveals that double-pass solar air heaters with counter flow arrangements show promising results. Note that the effect of curved design of channel in counter flow arrangements is yet to be reported. The study of surface-modified absorber with asymmetrically attached rib and its arrangement in curved designs with counter-flow double-pass solar air heaters (see Fig.4.1) is rare in literature. Counter-flow curved DPSAH is yet to be investigated in detail for its thermal performance for various design configurations. The novel part of this investigations is the new design of counter flow curved double-pass SAH has been reported which shows higher thermal performance than previously reported in parallel flow curved design.

The objectives of this paper are three-fold: first, to develop the computational models of smooth curved SPSAH, smooth parallel curved DPSAH, smooth counter curved DPSAH, roughened parallel curved DPSAH, and roughened counter curved DPSAH. Second, generate accurate data for the above designs for further analysis and determine the best design configurations (i.e., counter flow curved DPSAH) that show higher thermo-hydraulic performance. Third, establish functional relation for Nu and f from the data in terms of flow and design parameters, i.e., (Re and d/H) for the best design configuration. The correlations thus developed can predict the flow and heat transfer characteristics and facilitate further research and development of efficient solar air heaters. No such correlation exists in the literature that can estimate the performance characteristics of a counter flow curved SAH.

4.2 Computational fluid dynamics model

A two-dimensional computational model was developed for smooth and roughened curve DPSAH in ANSYS-FLUENT commercial software. Details of the numerical domain, boundary conditions, mesh generation, time and grid-independent study, governing equation, and experimental validation are described in the following subsection:

4.2.1 Description of numerical domain and operating parameters

The numerical domain of smooth and roughened curve SAHs consists of the rectangular duct flow passage. All SAHs have a top transparent glass surface, which allows the solar radiation to fall on the absorber surface of length (L), insulating the bottom wall and an inlet and outlet section through which air enters and exits (Fig.4.1). In parallel curved DPSAH, the fluid enters through the inlet section and distributes equally in the upper and lower channel, and finally exits from the outlet section. While in counter curved DPSAH, fluid enters from the inlet section of the upper duct and comes out from the outlet section of lower duct The total mass flow rate in parallel curved DPSAH is equal to the inlet mass flow rate in counter curved DPSAH. The length (L), curvature angle (α), and duct height (H) of SAH are taken 1600 mm, 25°, and 40 mm,

Table 4.1: Relevant literature on double pass solar air heater have various shapes of absorber plate, extended surface and flow pattern.

Author	Type of SAH	Absorber plate		Findings
		Nature	Extended surface	
Abdullah et al. [2]	Counter DPSAH, SPSAH	Flat	Aluminum cans	The daily thermal efficiency of staggered, aligned, flat DPSAHs was 30%, 26% and 10% respectively, at 0.05kg/s over the SPSAH.
Hernandez andQuinonez [45]	Parallel DPSAH, Counter DPSAH, SPSAH	Flat	-	Counter DPSAH has higher total useful energy gain as compare toParallel DPSAH and SPSAH.
Dhiman et al.[26]	Counter DPSAH, Parallel DPSAH	Flat	Wire matrix	Parallel DPSAH with packed bed was less efficient compare to Counter DPSAH with packed bed in term of thermal efficiency.
Kumar et al.[74]	Parallel DPSAH, SPSAH	curve	Semicircular and circular	A parallel DPSAH with asymmetric semicircular rib is thermally more efficient than that with symmetric circular rib.
Karim et al.[67]	Counter DPSAH, SPSAH	V-groove	-	The metrological and flow parameter has comparable effect on the overall performance of single and double flow SAH whilst the impact of geometrical parameters deviates appreciably in comparison to single pass configuration.
Singh & Singh[123]	SPSAH, Counter DPSAH	Flat, Curve	-	The air outlet temperature of CPDP(curve plate double pass) and CPSP (curve plate single pass) was higher compare to FPDP .(flat plate double pass) and FPSP (flat plate single pass) respectively.
Naphon.[98]	Counter DPSAH	Flat	Porous media	A Counter DPSAH with porous media has 29.5% higher thermal efficiency than that without porous media.
Singh et al.[129]	Counter DPSAH	Corrugated wavy	(Wire-mesh) porous media	Jet impingement: For the same flow rate, 40- and 80-holesabsorber surfacehas a of maximumthermal efficiency of 96.4% and 73.5%, respectively.
Ravi & Saini [114]	Counter DPSAH, SPSAH	Flat	V-shape	The maximum enhancement in Nuand f for roughened counter DPSAH were4.52 and 3.13 times respective more than compared to smooth counter DPSAH.

Table 4.2: Range of geometrical and operating parameters.

Geometrical and operating parameters	Range
Absorber plate length, L	1600 mm
Height of duct, H	40 mm
Hydraulic diameter of duct, D	77 mm
Rib diameter, d	4,6,8 and 10 mm
Rib pitch, P	30 mm
Location of absorber plate from glass , y	20 mm
Relative roughness height, d/H	0.1, 0.15, 0.20 and 0.25
Relative roughness pitch, P/H	0.75
Relative location of absorber plate, y/H	0.5
Rib shape, S	Semicircular
Uniform heat flux, q	800 W/m^2
Reynolds number, Re	5000 - 10000 (6 values)
Prandtl number, Pr	0.72
Curvature angle, α	25°
Channel width of duct, W	1000 mm

respectively, such that it has an identical surface area.The roughened parallel curved DPSAH and roughened counter curved DPSAH are shown in Fig.4.1.The semicircular ribs are equipped on both surfaces (up and down) of the absorber plate asymmetrically in both designs.The geometrical parameters of ribs are defined in terms of relative roughness height (d/H) and relative roughness pitch (P/H =0.75). Six and four different values of Re (5000-10000) and relative roughness pitch (d/H = 0.1-0.25) have been considered, respectively. All SAHs are simulated under similar geometrical and operating conditions. The detailed geometrical and operating parameters used in this numerical study are listed in Table 4.2.

4.2.2 Boundary condition

A constant solar radiation flux (q) 800 W/m2 falls on the absorber plate. The bottom wall has been kept in adiabatic wall condition. Velocity inlet, pressure outlet, and no-slip with impermeable boundary conditions have been applied at the inlet section, outlet section, and walls of the SAH duct, respectively. A combined convection and radiation heat transfer coefficient ($h = 5 + 3.8V_\infty$) was imposed on the top transparent surface of SAH[74]. Initially, air enters at constant velocity with temperature 300 K, and its initial temperature within the computational domain was also taken as 300 K. As SAHs operates at low and moderate temperature range between 40°C to 100°C and in this range changes in thermophysical properties of air are insignificant [22, 24],and therefore, in present study thermophysical properties of the air are assumed constant. The thermophysical and optical properties of air, glass and absorber plate are given in Table 4.3.

Table 4.3: Properties of materials for numerical simulation [6, 74].

Properties	Symbol	Air	Absorber (Aluminum)	Glass
Density, (kg/m^3)	ρ	1.184	2702	2500
Thermal conductivity, (W/m-K)	K	0.026	273	1.2
Specific heat, (J/kg-K)	Cp	1003	903	800
Dynamic viscosity, (N.s/m^2)	μ	1.855×10^5	-	-
Emissivity	ε	-	0.9	0.88
Refractive index	n	-	1	1.53

4.2.3 Governing equation

The governing equation of working fluid flow through the SAH duct are obtained by using the principle of conservation of mass, momentum and energy. The Navier–Stokes equations govern the velocity and pressure of the fluid flow. Since the flow is turbulent, each velocity component is decomposed into a mean part and a fluctuating part. The non-linear Reynolds-averaged Navier–Stokes (RANS) equations are obtained after averaging, which govern the mean flow as mentioned below. The equations contain only the mean velocity and pressure term as Reynolds stresses are expressed as a function of the mean flow and hence, no reference to fluctuating part of velocity appears in the final equation.

Continuity equation or Mass conservation[74]:

$$\frac{\partial \rho}{\partial t} + \frac{\partial (\rho u_i)}{\partial x_i} = 0 \tag{4.1}$$

Navier-stokes or momentum conservation equation[116]:

$$\frac{\partial (\rho u_i)}{\partial t} + \frac{\partial (\rho u_i u_j)}{\partial x_j} = -\frac{\partial P}{\partial x_i} + \frac{\partial}{\partial x_j}\left[\mu\left(\frac{\partial u_i}{\partial x_j} + \frac{\partial u_j}{\partial x_i}\right)\right] + \frac{\partial}{\partial x_j}\left(-\rho\overline{u_i' u_j'}\right) + \rho g_i \tag{4.2}$$

where the term $-\rho\overline{u_i' u_j'}$ is the Reynold constrained and it can be written as[6]:

$$-\rho\overline{u_i' u_j'} = \mu_t\left(\frac{\partial u_i}{\partial x_j}\right) \tag{4.3}$$

Energy conservation equation:

$$\frac{\partial (\rho T)}{\partial t} + \frac{\partial (\rho u_i T)}{\partial x_i} = \frac{\partial}{\partial x_j}\left[(\Gamma + \Gamma_t)\frac{\partial T}{\partial x_j}\right] \tag{4.4}$$

where, $\Gamma = \frac{\mu}{Pr}$ and $\Gamma_t = \frac{\mu_t}{Pr_t}$ in which Pr_t is the turbulent prandtl number, μ_t denote turbulent dynamic viscosity, Pr and μ denote laminar prandtl number and dynamic viscosity, respectively. The realizable k-ε turbulence model is used in this study and the equation for turbulent kinetic energy (k) and turbulent dissipation rate (ε) for numerical analysis are given as [139, 151]:

$$\frac{\partial(\rho k)}{\partial t} + \frac{\partial(\rho u_i k)}{\partial x_i} = \frac{\partial}{\partial x_j}\left[\left(\mu + \frac{\mu_t}{\sigma_k}\right)\frac{\partial k}{\partial x_j}\right] + G_k + G_b \tag{4.5}$$

$$\frac{\partial(\rho\varepsilon)}{\partial t} + \frac{\partial(\rho u_i \varepsilon)}{\partial x_i} = \frac{\partial}{\partial x_j}\left[\left(\mu + \frac{\mu_t}{\sigma_\varepsilon}\right)\frac{\partial \varepsilon}{\partial x_j}\right] - \rho C_{2\varepsilon}\frac{\varepsilon^2}{k+\sqrt{\nu\varepsilon}} - C_{1\varepsilon}\frac{\varepsilon}{k}C_{3\varepsilon}G_b \tag{4.6}$$

Turbulent dynamic viscosity (μ_t) is calculated by using the formula

$$\mu_t = \rho C_\mu \frac{k^2}{\varepsilon} \tag{4.7}$$

where the values of $C_{1\varepsilon}$, $C_{2\varepsilon}$,$C_{3\varepsilon}$, C_μ, σ_k and σ_ε are 1.44, 1.92, -0.33, 0.09, 1.0 and 1.3 respectively. G_k and G_b denotes the production of turbulent kinetic energy due mean velocity gradient and buoyancy, respectively.

Discrete ordinates method has been used to model the radiation part of the heat transfer[11]:

$$\nabla.\left(I\left(\vec{r},\vec{s}\right)\vec{s}\right) + (a+\sigma_s)\,I\left(\vec{r},\vec{s}\right) = an_r^2\frac{\sigma T^4}{\pi} + \frac{\sigma_s}{4\pi}\int_0^{4\pi} I\left(\vec{r},\vec{s}\right)\varphi\left(\vec{s},\vec{S'}\right)d\omega \tag{4.8}$$

where absorption coefficient (a)(a), scattering coefficient (σ_s), refractive index (n) and phase function (φ) are assume independent of wavelength.

4.2.4 Performance parameters

In order to estimate the value of Nu and $f$for different designs of SAHs, the data of mass flow average air outlet temperature(T_0), surface average absorber plate temperature (T_P), and pressure drop across the duct are collected. The average bulk mean temperature (T_{bm})of working fluid flowing through the SAH is defined as:

$$T_{bm} = \frac{(T_0 + T_i)}{2} \tag{4.9}$$

Total useful heat gains of working fluid is determined by applying 1st law of thermodynamics.

For parallel DPSAH

$$Q_u = \dot{m}_l C_P (T_{l0} - T_i) + \dot{m}_u C_P (T_{u0} - T_i) \tag{4.10}$$

For counter DPSAH

$$Q_u = \dot{m} C_P (T_0 - T_i) \tag{4.11}$$

where $\dot{m} = m_l \dot{+} \dot{m}_u$

The average convective heat transfer coefficient between absorber wall and flowing air inside the SAH is determined as

$$h = \frac{Q_u}{A_{eff} (T_P - T_{bm})} \tag{4.12}$$

The average value of Nusselt number is determined as

$$Nu = \frac{hD_h}{K} \tag{4.13}$$

The hydraulic diameter of SAH is defined as

$$D_h = \frac{4A_c}{p} \tag{4.14}$$

The average value of friction factor is calculated by using Darcy-Weisbach equation

$$f = \frac{\triangle P D_h}{2\rho L V^2} \tag{4.15}$$

The nature of fluid flow behavior inside the curve SAH is determined by the essential dimensionless parameters Dean number (D_n) and Reynold number (Re). These parameters signify that fluid flow inside the curve solar air heater is either turbulent or laminar. In our study, the values of Re and $D_n$come under a turbulent regime[65].

Reynold number defined as

$$Re = \frac{\rho V D_h}{\mu} \tag{4.16}$$

And

Dean number related to Reynolds number as

$$D_n = Re\sqrt{\frac{D_h}{2R_c}} \tag{4.17}$$

Strength of turbulence inside the duct is determined by turbulent intensity (I). It is defined as [33]

$$I = 0.16Re^{-0.125} \tag{4.18}$$

Thermal hydraulic efficiency of solar air heater is determined as

$$\eta_{the} = \frac{Q_u - P_{fan}}{IA_{eff}} \tag{4.19}$$

4.2.5 Mesh description, grid independence and time independence

A finite volume technique was used to discretize the 2D numerical domain. An unstructured triangular shape element has been used to meshing the flow domain. A very fine and coarse element was created near the absorber wall, ribs, and away from the walls, respectively, as shown in Fig.4.2, to capture the boundary layer gradient and save computational time. Structure mesh has lesser ability to capture primary and secondary eddies near the ribs region than unstructured mesh [35, 125].

4.2.5.1 Mesh independence study

To ensure the outcome of SAH is independent of the variation of grid size, a grid-independent study was performed. For this study, the number of elements was varied from 278800 to 503610 in four steps. These four-grid distributions were performed on roughened counter curved DPSAH with a d/H value of 0.20 and a constant value of Re and P/H of 5000 and 0.75, respectively. The variation of Nusselt number (Nu), outlet air temperature (T_0), and their percentage difference with the number of elements are presented in Table4.4. It can be observed that as the number of elements changes from 401078 to 503610, the percentage changes in the values of Nu and T_0 are less than 0.5%. Therefore, 401078 elements were chosen for all the cases considered in this study.

4.2.5.2 Time independent study

Time independent study was performed by using 401078 elements for roughened counter curved DPSAH at Reynolds number 5000 for fixed value of d/H and P/H of 0.20 and 0.75 respectively.

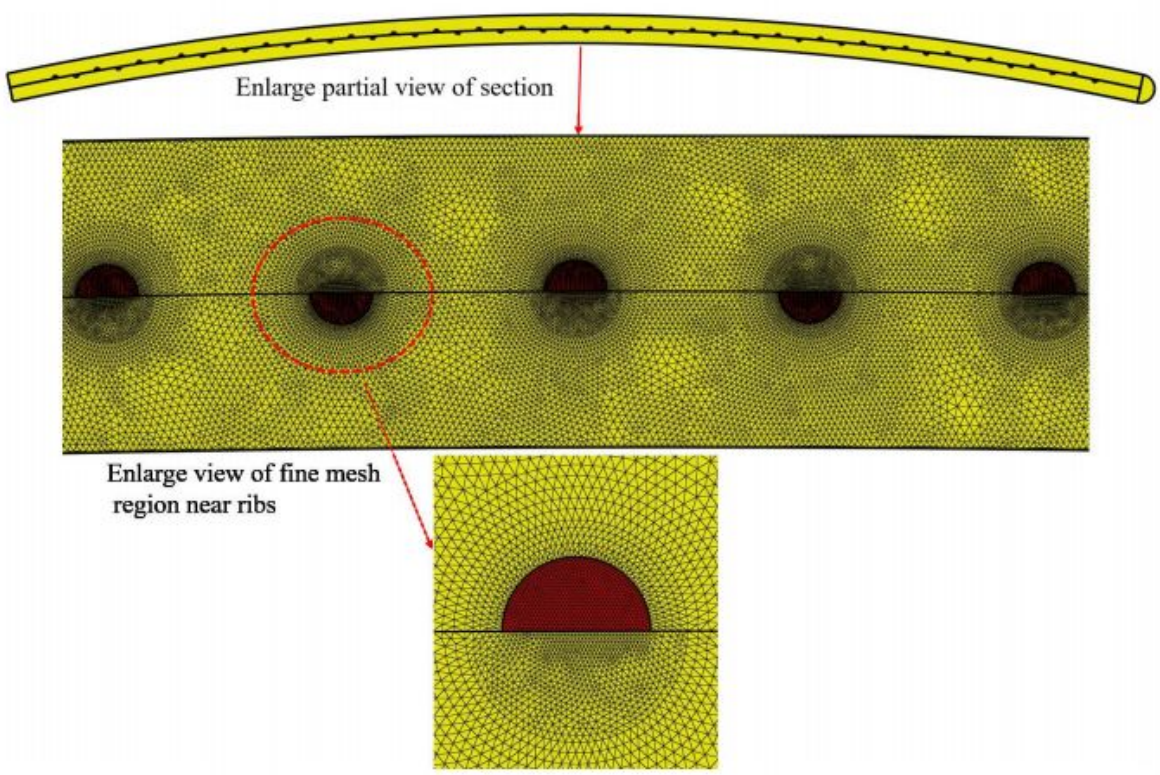

Figure 4.2: Mesh of a curve roughened counter DPSAH equipped with asymmetric semicircular turbulators.

Table 4.4: Grid independent study

Number of elements	Nusselt number, Nu	% Difference	Outlet air temperature T_0, (K)	% Difference
278800	30.68	-	329.29	
347028	31.05	1.20	328.17	0.34
401078	31.31	0.81	327.7	0.14
503610	31.32	0.03	327.66	0.01

Three time steps were chosen to perform time independent study which is presented in Table 4.5. When time step changes from 0.125 to 0.0625, the percentage variation in Nu and T_0 have been found less than 0.5%. Based on the above discussion, time step of 0.125 was selected for further investigation.

4.2.6 Validation with experimental results

The validation of the numerical model has been performed by matching results with the experimental results of Mahboub et al.[87]. The computational domain and experimental setup have the exact dimensions as reported in the literature[87]. It was assumed that flow is steady and density of fluid is a function of temperature. A convection boundary condition has been

Table 4.5: Time independent test

Time step (second)	Number of elements	Nusselt number	% Difference	Outlet air temperature	% Difference
0.25		30.93	-	325.34	-
0.125	401078	31.31	1.21	327.7	0.73
0.0625		31.35	0.12	328.1	0.13

Table 4.6: Experimental validation of pressure drop across the curve SAHs

Mass flow rate (kg/sm^2)	Pressure drop across the duct in experimental study (N/m^2)	Pressure drop across the duct in numerical study (N/m^2)	% in errors
0.017	46.7	44.5	4.71
0.029	122.93	119.83	2.52
0.047	303.19	298.68	1.48

employed at the glass cover's top surface to consider combining convection and radiation heat loss through the glass. Mass flow inlet and pressure outlet boundary conditions were assigned at the inlet and outlet of the computational domain. The numerical simulations have been performed for each mass flow rates of 0.0172, 0.029, and 0.0472 kg/sm^2 for the heat flux range 800-1000 W/m^2. The Reynolds number evaluated from these mass flow rates comes under the turbulence regime. Therefore, the turbulence model (realizable k-epsilon) was used for turbulence modelling. The results of numerical simulation (outlet temperature and pressure drop) were recorded. The variation of outlet air temperatures from numerical and experimental results is shown in Fig.4.3 for m=0.0172 kg/sm^2. Note that outlet temperature increases with the increase of solar radiation flux. It has a 9.4% average absolute deviation from experimental outcomes, which comes under acceptable limit. The percentage deviation in outlet air temperature was evaluated as follow:

$$Relativeerror = \frac{(T_0 - T_i)_{numerical} - (T_0 - T_i)_{experimental}}{(T_0 - T_i)_{experimental}} \tag{4.20}$$

The variation of pressure drop across the curve SAH with respect to mass flow rate for experimental and numerical analysis is listed in Table4.6. The maximum error of 4.71% appears between experimental and numerical results of pressure drop across the curve SAH. Since the numerical results closely predict the experimental data, the said numerical model is validated and it can be used for further design studies.

4.3 Results and discussion

The flow behavior and heat transfers of two categories of curve solar air heater shown in Fig.4.1 have been discussed. Their thermo-hydraulic characteristic was reported in terms of effectiveness, Nu, and f for the range of Re and d/H values of $5000-10000$ and $0.1-0.25$, respectively. The numerical simulations of curve solar air heaters with parallel and counter flow arrangement having an absorber surface, smooth (without ribs) and rough (with asymmetric semicircular ribs above and below) have been performed

4.3.1 Performance comparison: counter vs. parallel curved DPSAH

4.3.1.1 Thermal performance of smooth curved SAHs

Figure4.4 depicts the effect of Re variation on Nu at various study cases (smooth counter curved DPSAH, smooth parallel curved DPSAH, and smooth curved SPSAH). As SAHs have a curved nature flow passage, centrifugal force dislocates the maximum value of flow velocity toward the absorber, creating secondary vortices in the channel cross-section. The strength of secondary vortices and the mean velocity of working fluid increases with increase in Re. Consequently, turbulent intensity inside the duct enhances significantly. As a result, the growth of the thermal boundary layer thickness near the absorber surface reduces, which enhances the heat transfer rate from absorber surface to working fluid and reduce the temperature of absorber plate. For smooth counter curved DPSAH, there is an augmentation in Nu at $Re = 5000$ by about 23 and 44 compared to smooth parallel curved DPSAH and smooth curved SPSAH, respectively. For smooth parallel curved DPSAH, Nu enhancement is 17as compared to smooth curved SPSAH. The average Nu of smooth counter curved DPSAH (double heat transfer area, minimum top loss) is higher than that of smooth parallel curved DPSAH (double heat transfer area, medium top loss) and smooth curved SPSAH (maximum top losses). It establishes that smooth counter curved DPSAH performs better than smooth parallel curved DPSAH and smooth curved SPSAH. A similar observation was given by Abdullah et al.[2] in their experimental study, although counter DPSAH design and operating parameters differed from the present study.

Figure4.5 presents the temperature variation across the duct height at mid-section of smooth counter and smooth parallel curved DPSAH for a fixed value of Re. It is noticed that the temperature of flowing fluid increases along with the duct height and reached maximum at the half size of the duct (i.e., absorber position) and then after it decreases. However, the bulk mean temperature of working fluid within the channel (upper and lower) is higher in smooth counter curved DPSAH. In contrast, the portion of the fluid in contact with the absorber surface has a higher temperature value in smooth parallel curved DPSAH. Consequently, more top heat losses to surrounding in smooth curved parallel design as compare to counter curved design. This is because the mass of fluid in counter curved DPSAH does not split, unlike in smooth parallel

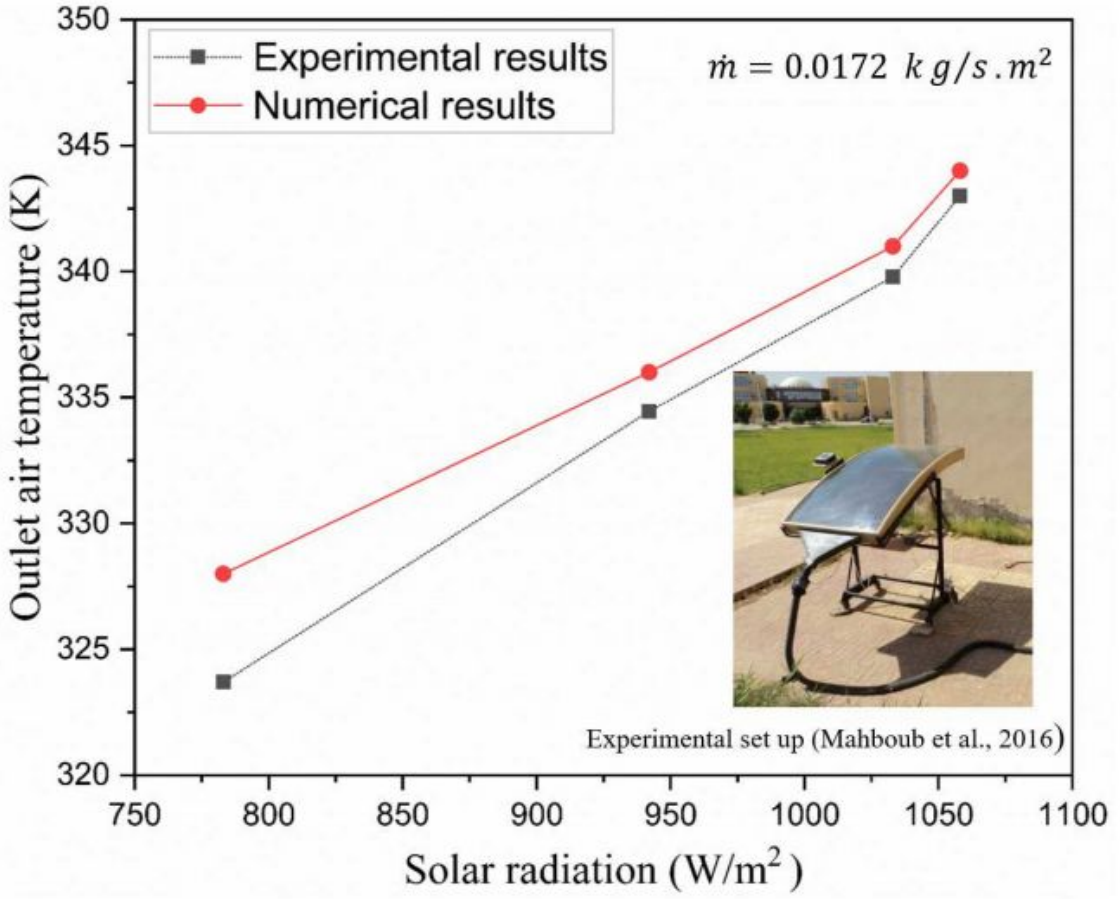

Figure 4.3: Comparison of experimental and CFD results of outlet air temperature w.r.t solar radiation.

curved DPSAH. Further, higher turbulence occurs in both the channel and fluid cover longer distance in counter design as compare to parallel design. Thus, more temperature difference between the absorber and the environment is achieved in smooth parallel instead of smooth counter curved DPSAH. Consequently, more top heat losses to surrounding in smooth parallel design is observed as compare to counter curved DPSAH.

Table4.7 summarized the thermal efficiency. Note that counter designs with curved double pass SAH have the efficiency which is almost double than single curved SAH. This is due to low top losses and double effective heat transfer area of the absorber in smooth curved counter DPSAH compared to smooth curved SPSAH.

4.3.1.2 Thermal performance of roughened curved SAHs

The variation of d/H with Nu for various case studies (roughened counter and roughened parallel curved DPSAH) for a constant P/H and Re of 0.75 and 10000, respectively, has been illustrated in Fig4.6. It is seen that the values of Nu rise with increase in d/H. Moreover, the

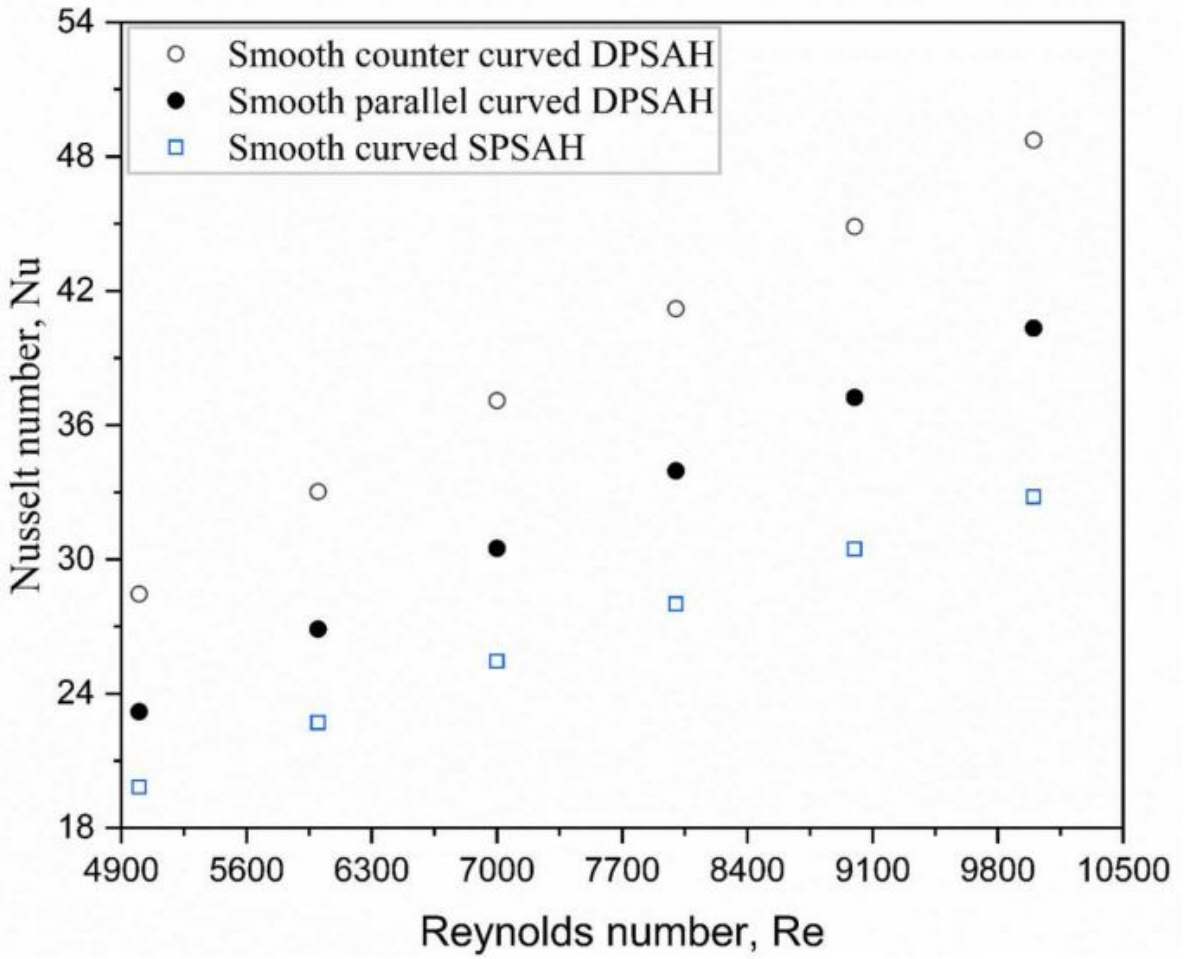

Figure 4.4: A plot of Nu with respect to Re at a constant heat flux.

Table 4.7: Thermal hydraulic efficiency comparison among smooth curved designs SAHs.

Reynold number	Smooth curved SPSAH	Smooth counter curved DPSAH
5000	0.365	0.731
6000	0.367	0.734
7000	0.368	0.739
8000	0.369	0.741
9000	0.371	0.742
10000	0.376	0.744

maximum percentage increase of 19-23% in Nu is found in the roughened counter compared to roughened parallel curved DPSAH. An improvement in Nu is found due to longer residence time and an increase in turbulent kinetic energy (TKE), resulting in good inter-mixing of hot and cold fluid in the recirculation zone. This increase in TKE happen due to generation of vortices (primary and secondary) near ribs and curve nature of flow passage. Contours of TKE for these two designs (roughened counter and roughened parallel curved DPSAH) have been depicted in Fig4.7 at distinct values of d/H. It can be seen that a high TKE region is observed at the downward of ribs because a larger velocity gradient leads to an increase of TKE in the flow field. The length of the high TKE region in the direction flow and scale of TKE in Fig4.7 increases with growing relative roughness height. The high strength of TKE between the consecutive turbulators signifies higher heat transfer from the collector surfaces. High Nu in counter flow designs as shown earlier corroborates these observations. Many researchers in their studies found a similar observation, but they used different operating parameters and geometrical configurations of turbulators in SAHs[35, 114, 139].

Figure 4.9 shows the variation of thermal effectiveness concerning relative roughness height for roughened SAHs at a constant value of Re and P/H of 10000 and 0.75, respectively. The results indicate thermal effectiveness increases with higher values of d/H. As asymmetric semicircular ribs are attached on both sides of the absorber surface, they disturb the development of the boundary layer, and generate primary and secondary recirculation regions upstream and downstream across the ribs. This causes augmentation in TKE and turbulent intensity (I). Consequently, the heat loss rate from the hot absorber wall to the core cold fluid is enhanced. Moreover, with growing d/H, the size of recirculation zone, exchange of momentum of fluid with absorber and level of TKE in the SAH duct are enhanced, and subsequently, the heat transfer rate from the absorber surface to the cold fluid increases. With enhanced heat transfer rate, outlet air temperature increases, and absorber surface temperature declines. Thus, thermal effectiveness increases with growing values ofd/H. The values of thermal effectiveness of roughened counter curved DPSAH are larger than that of roughened parallel curved DPSAH. This is because the absorber surface temperature of roughened parallel curved DPSAH is greater than that of roughened counter curved DPSAH, which can be seen with temperature contour (see in Fig 4.8). The maximum percentage increase of 32-37% in thermal effectiveness is found in the roughened counter compared to roughened parallel curved DPSAH.

Figure 4.8 shows the temperature contour of roughened counter and roughened parallel curved DPSAH for fixed valueRe and d/H of 10000 and 0.25, respectively. The results indicate that roughened counter curved DPSAH has a lower absorber surface temperature than roughened parallel curved DPSAH. Moreover, the heat extraction rate by moving fluid in an upper and lower duct of roughened parallel curved DPSAH are equal. In contrast, the heat removal rate by the working fluid in the channels, above and below the absorber surface of roughened counter curved DPSAH is higher and lower, respectively. This is because the mass of flowing air in the

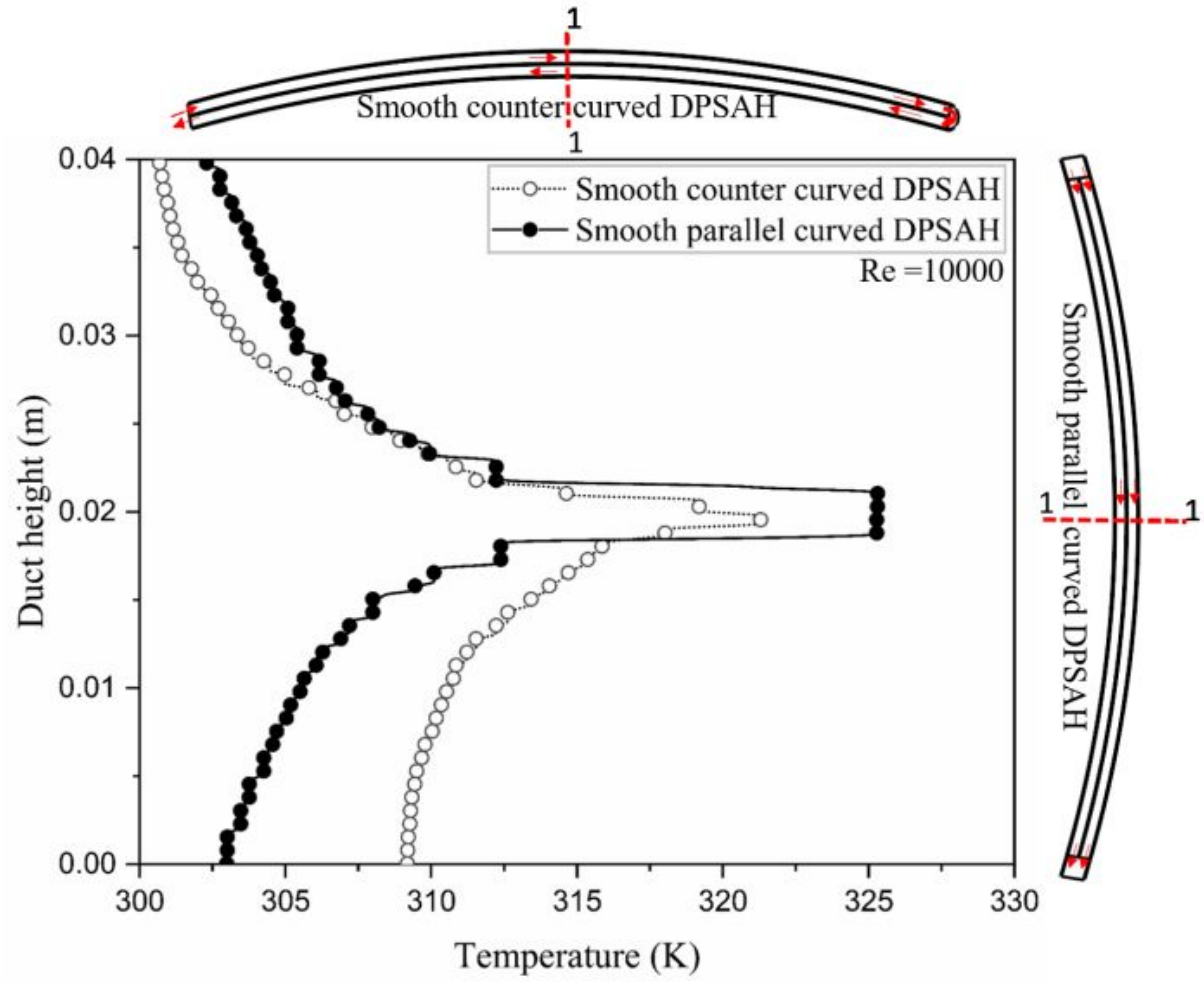

Figure 4.5: Air temperature distribution along the duct height at mid-section of smooth counter and smooth parallel curved DPSAH at Re = 10000.

upper channel of roughened counter curved DPSAH is large compared to roughened parallel curved DPSAH due to splitting of mass of flowing air in roughened parallel curved DPSAH. Attaching unsymmetrical turbulators on both sides of the absorber facilitates the intense mixing and generated asymmetrical vortices above and below the absorber plate. These vortices entrain colder fluid from the outer region. Higher absorber surface temperature indicates higher heat loss to the environment because of temperature discrepancy between the absorber plate and sky. This top loss degrades the thermal performance of SAHs. Higher the top loss indicates the lower thermal performance of SAHs.

Figure 4.11 shows the influence of varying relative roughness height (d/H) on the thermal-hydraulic efficiency of roughened counter and parallel curved DPSAH for a fixed value of Re and P/H of 10000 and 0.75, respectively. It is noticed that thermal-hydraulic efficiency increases with an increase of d/H. The effect of the d/H ratio is more pronounced in counter design. This is because the fluid in roughened counter curved DPSAH has maximum inlet velocity, which ex-

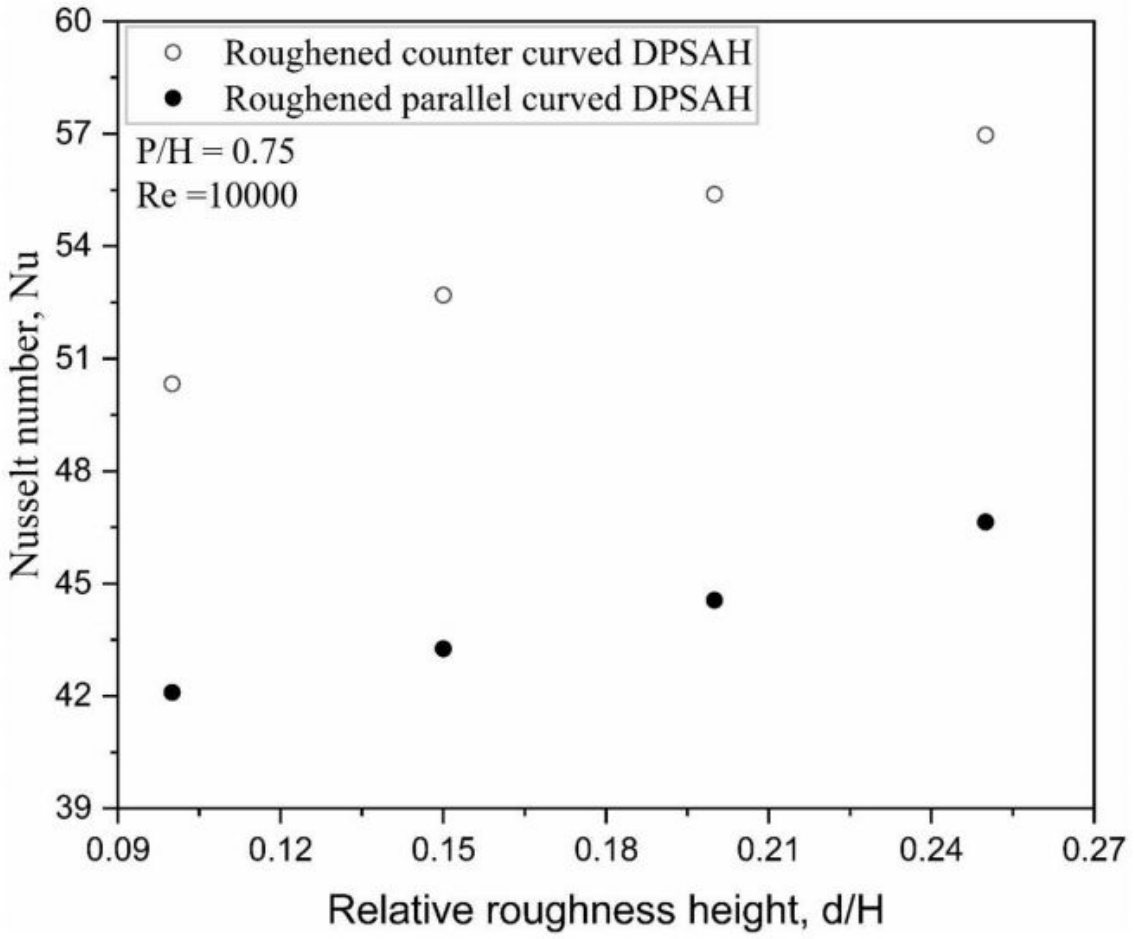

Figure 4.6: Effect of d/H on Nu for counter and parallel curved DPSAH for a constant value of Re and P/H.

changes the momentum around ribs and absorber surfaces, produces a larger recirculation zone across the ribs, and travels longer path length. As a result, an augmentation in local heat transfer coefficient, mixing process between cold and hot fluid, and more extended heat removal from the absorber to working fluid is observed. Consequently, maximum heat transfer occurs and reduces the temperature of the absorber surface. Thus, a minimum temperature difference between absorber and sky is achieved. Consequently, roughened counter curved DPSAH has minimum top loss compared to roughened parallel curved DPSAH.

4.3.1.3 Hydraulic performance of curved SAHs

Figure 4.12 shows the local wall shear stress variation along with the absorber length in upper duct of roughened counter and roughened parallel curved DPSAH for a fixed value of Re and d/H of 10000 and 0.75, respectively. The peaks are seen in the figure at the semicircular ribs, which show higher shear stresses. The first peak depicts the extreme value of wall shear stress

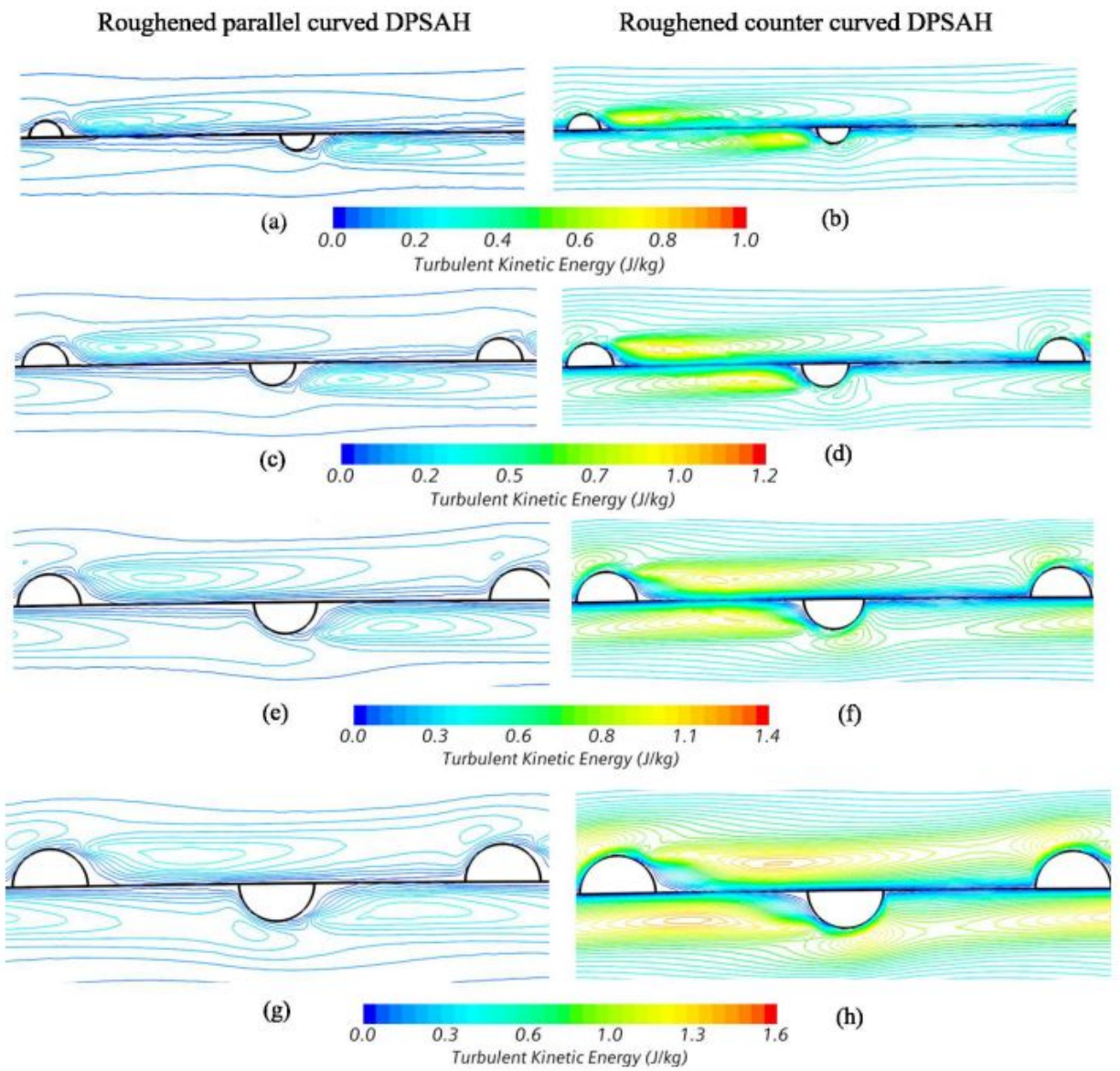

Figure 4.7: Contours of TKE of roughened counter and parallel curved DPSAH at $Re = 10000$ for a constant valueP/H and distinct values of relative roughness height (a) $d/H = 0.1$, (b) $d/H = 0.1$, (c) $d/H = 0.15$, (d) $d/H = 0.15$, (e) $d/H = 0.20$, (f) $d/H = 0.20$, (g) $d/H = 0.25$ and (h) $d/H = 0.25$, flow is from left to right.

due to a greater momentum exchange of fluid on the semicircular surface and the second peak appears due to the recirculation zone generated downstream of the rib in the direction of the flow field. Similar phenomena were also seen in numerical study of Menni et al.[94]. Besides, the maximum value of local wall shear stress is observed in roughened counter compared to roughened parallel curved DPSAH. Note that higher heat transfer rates are accompanied by higher shear stresses in the counter design of SAH. This can be better understood with the help of velocity contours, as illustrated in Fig 4.10. It is found that the magnitude of maximum velocity is observed in a roughened counter as compare to roughened parallel curved DPSAH. One reason

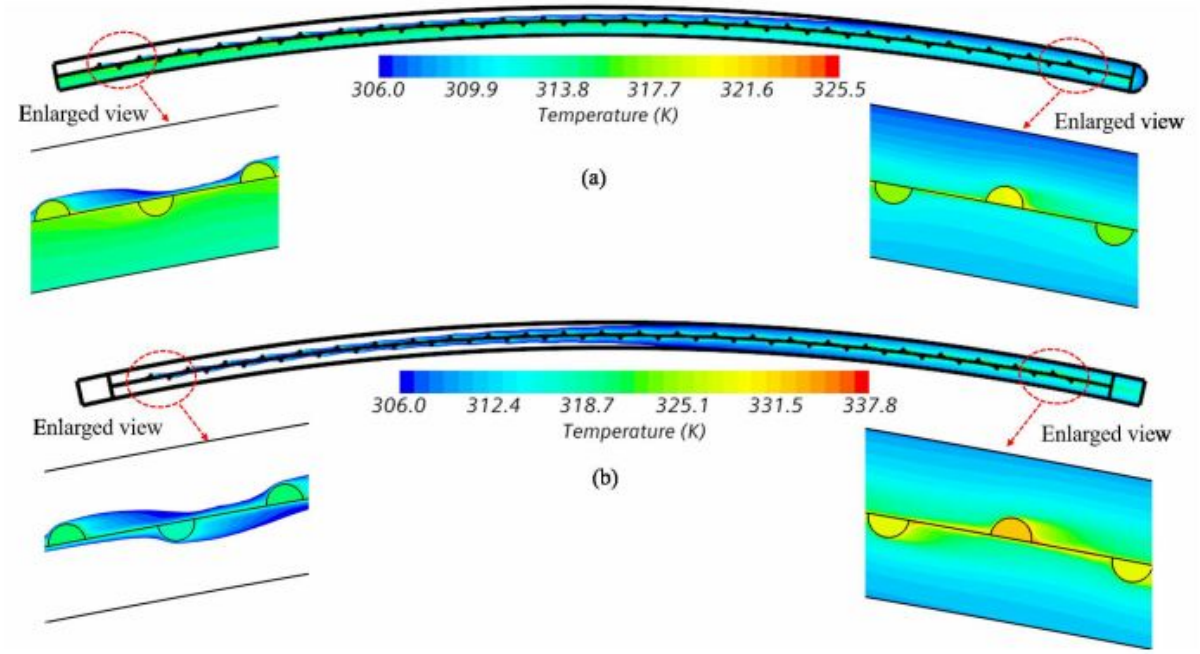

Figure 4.8: A contour plot of temperature for a constant value of Re and d/H of 10000 and 0.25 roughened (a) counter (b) parallel curved DPSAH.

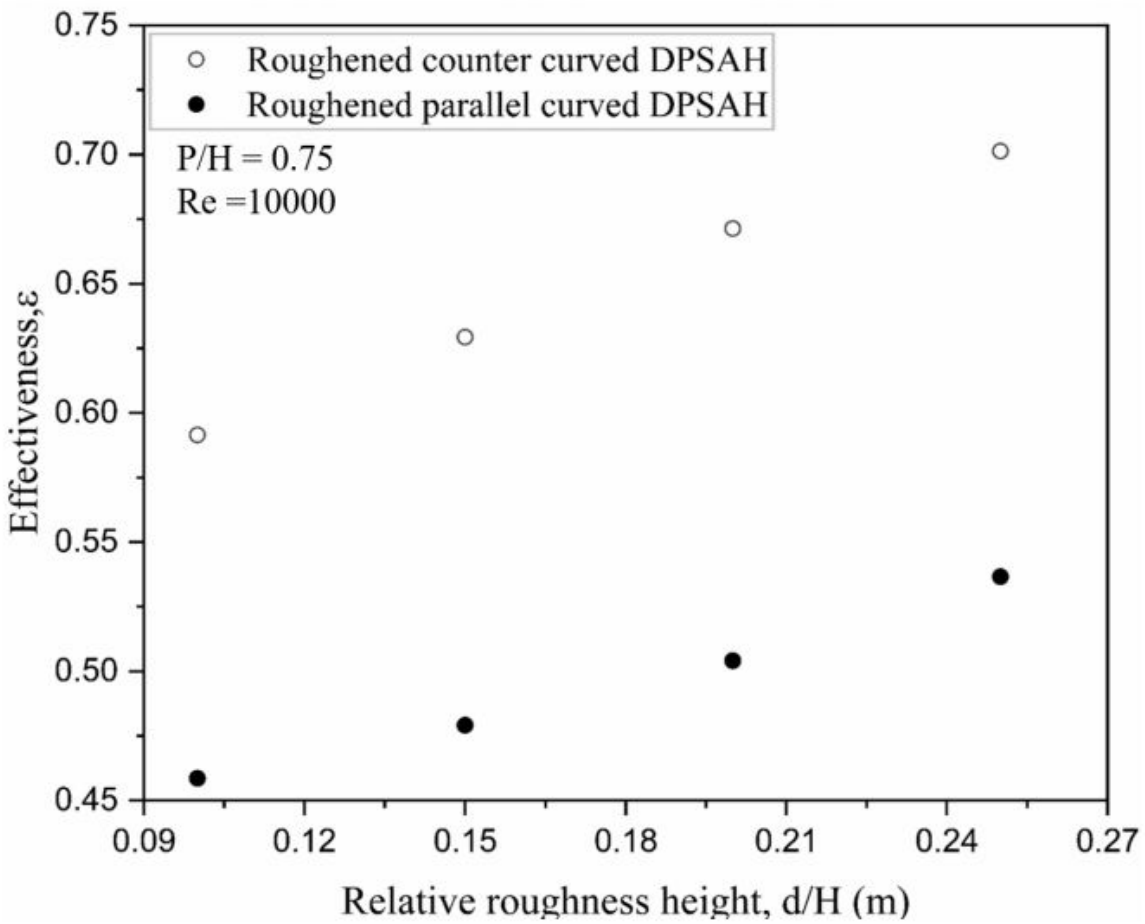

Figure 4.9: A plot of thermal effectiveness versus relative roughness height.

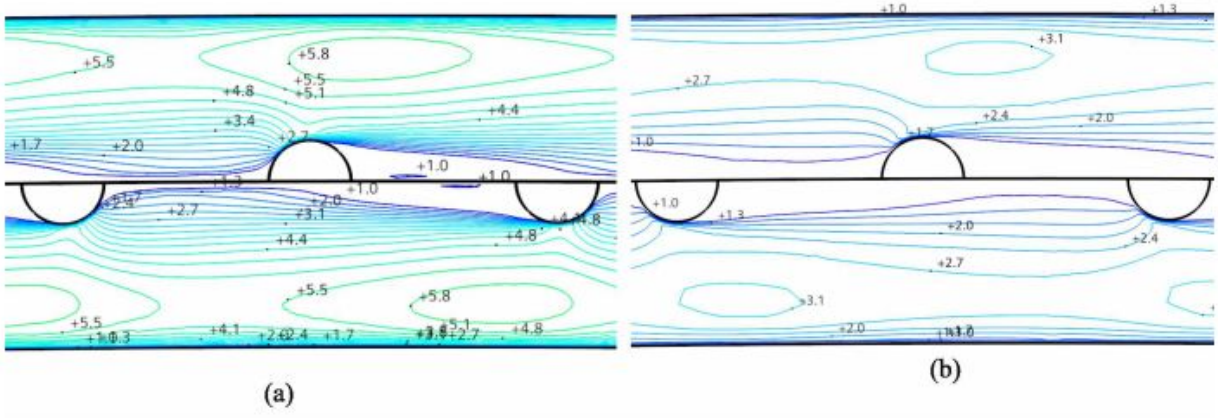

Figure 4.10: Contour of velocity magnitude at constant value of Re and d/H of roughened (a) Counter (b) Parallel curved DPSAH.

could be the higher mass flow rates in the counter design of SAH. Thus, maximum momentum exchange creates an extreme value of wall shear stress, therefore, roughened counter curved DPSAH has a larger magnitude of wall shear stress. With the increase in wall shear stresses, the pressure loss across the duct also multiplies. This pressure drop occurred due to obstruction created by ribs and increased passes length of the duct. Thus, the value of friction factor for the above investigated designs of SAHs in descending order are: roughened counter curved DPSAH > roughened parallel curved DPSAH > smooth counter curved DPSAH > smooth parallel curved DPSAH > smooth curved SPSAH. The maximum percentage increase of $9-18\%$ in friction factor has been observed for roughened counter curved DPSAH compared to roughened parallel curved DPSAH for a constant value of $Re = 10000$ and the range of values of $d/H(0.1-0.25)$. Since pressure drop or friction factor calculations are an essential performance parameter, a correlation has been developed in the next section.

It is now clear that the counter design of curved DPSAH performs thermally better than the parallel configuration of curved DPSAH. In the above study, only a few cases of geometric and flow parameters were presented. To facilitates the prediction for a wide range of parameters two new correlations have been developed as a function of Nu and f.

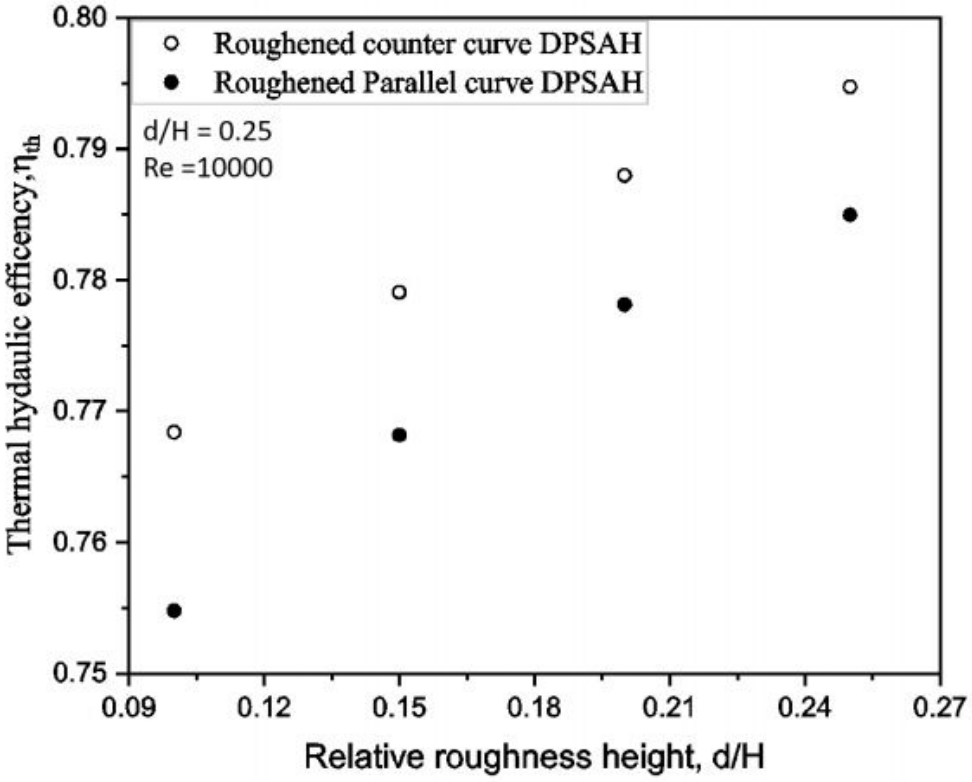

Figure 4.11: Effect of relative roughness height on thermal hydraulic efficiency for fixed value of Re and P/H of 10000and 0.75.

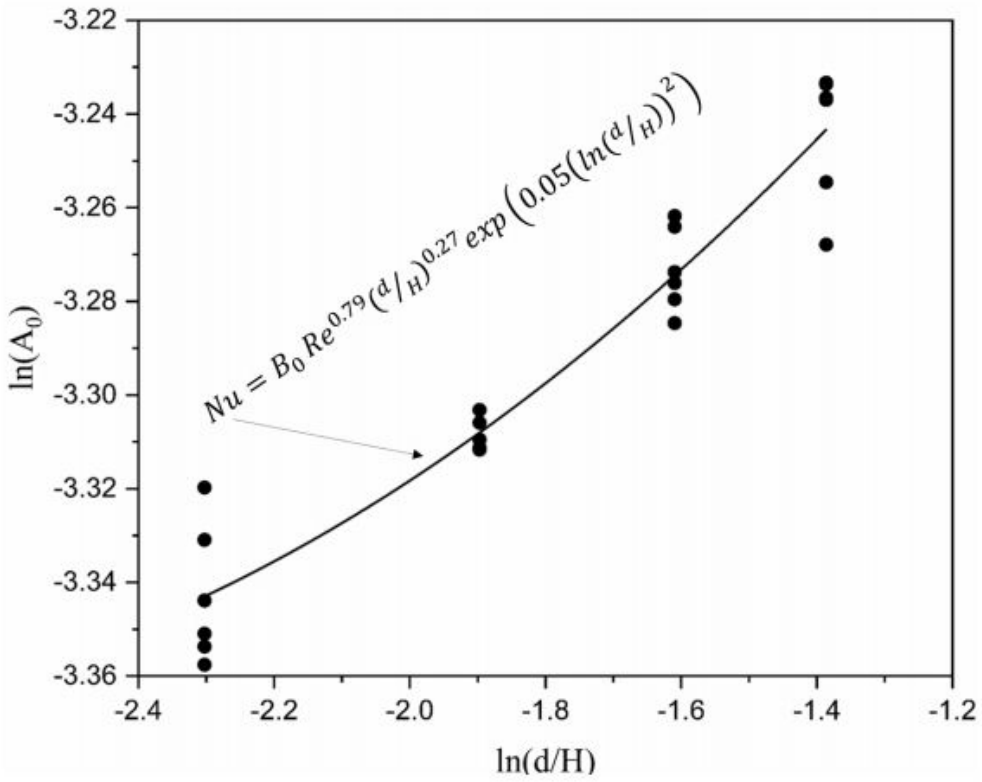

Figure 4.14: A plot of ln(A_0) vs ln(d/H)

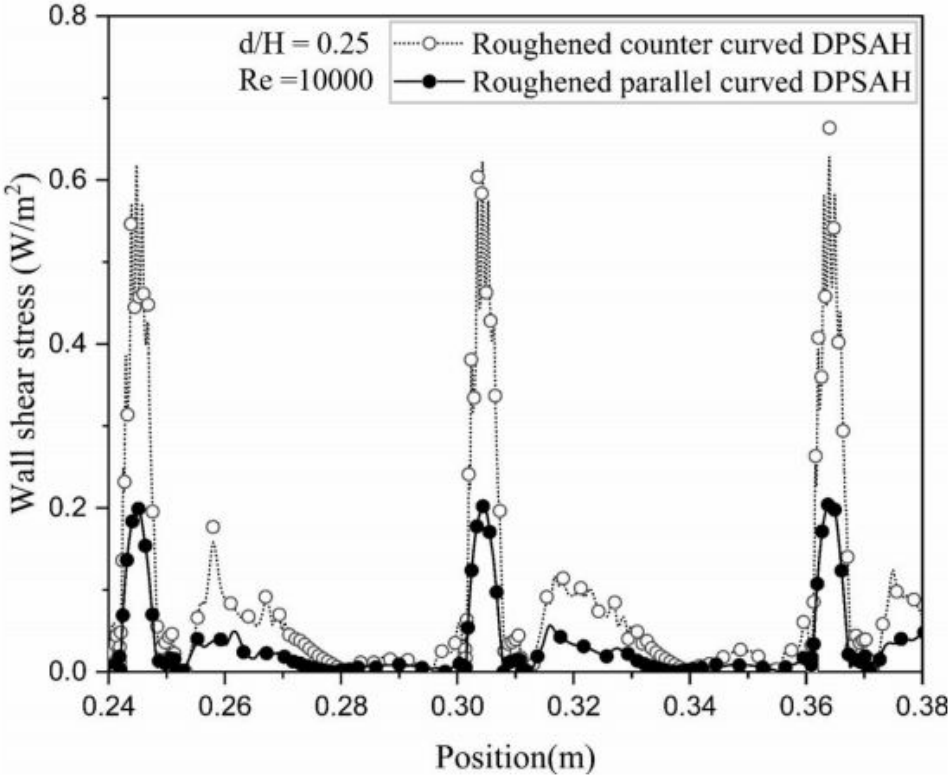

Figure 4.12: Variation of wall shear stresses with longitudinal length of absorber plate in roughened SAHs.

4.4 Development of correlation for Nu and f

The values of Nu and f varies with the values of Re and d/H. The functional relationship of these parameters can be written in term of Re and d/H as::

$$Nu = f_1(Re, d/H) \tag{4.21}$$

$$f = f_2(Re, d/H) \tag{4.22}$$

The functional form of function f_1 and f_2 are derived from the data obtained from the numerical model as presented before. These functional relationships have been established in term of roughness and flow parameters following the same procedure given by Kumar and Layek[75] .

4.4.1 Correlation for Nu

Values of Nu variation against the Re on a log-log scale is depicted in Fig 4.13. These data points fit into a straight line by using regression analysis and gives the following relation:

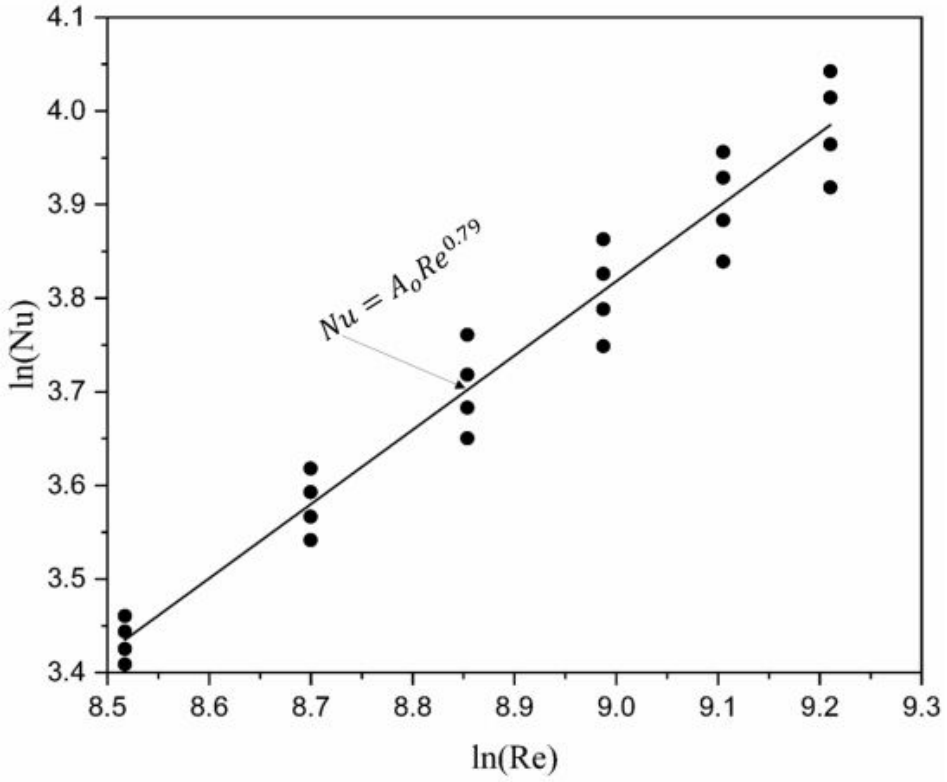

Figure 4.13: A plot of $\ln(Nu)$ vs $\ln(Re)$

$$Nu = A_0 Re^{0.79} \tag{4.23}$$

where A_0 also depends on another parameter, i.e., d/H. A plot of $ln(A_0)$ with respect to $ln(d/H)$ has been depicted in Fig 4.14. A second-order polynomial is fitted by using regression analysis and given as:

$$Nu = B_0 Re^{0.79} (d/H)^{0.27} exp\left[0.05\{ln(d/H)\}^2\right] \tag{4.24}$$

The values of coefficients obtained are

$A_0 = 0.036$ and $B_0 = 0.052$

Thus, the correlation for Nusselt number variation is

$$Nu = B_0 Re^{0.79} (d/H)^{0.27} exp\left[0.05\{ln(d/H)\}^2\right] \tag{4.25}$$

If Nu is function of D_n and d/H, then only the coefficient 0.052 will change to 0.32, and D_n in the above correlation replaces Re.

4.4.2 Correlation for f

The same method has been adopted to determine the functional relation for f in terms of Re and d/H. The coefficient values depend on the flow parameter and roughness parameter, as shown in Fig. 4.15-4.16.

The values of coefficient are

$C_0 = 0.62$ and $D_0 = 10.07$

The final correlation for friction factor is given by

$$f = 10.07 Re^{-0.26} (d/H)^{2.45} exp\left[0.49\{ln(d/H)\}^2\right] \tag{4.26}$$

If the above equation is written in term of Dean number (D_n) and relative roughness height (d/H) then only coefficient 10.07 will change to 5.53 and Re is replaced by D_n Figure 4.17-4.18 illustrates the comparisons between simulated values of Nu, f, and those obtained using the above formulated correlation. It is noted that the average absolute percentage error between numerical and predicted values of Nu and f are 1.8% and 0.52%, respectively. Since the correlations forecasts reasonably close values, the proposed relationship can be used to predict the thermal and hydraulic performance of a counter curved DPSAH.

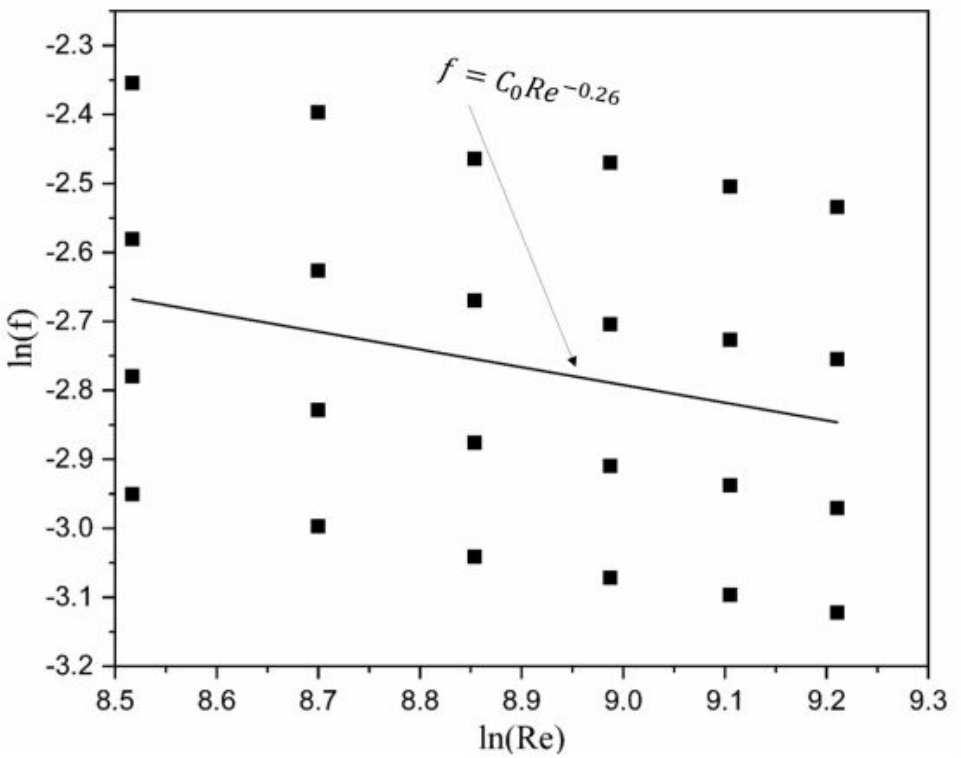

Figure 4.15: A plot of $\ln(f)$ vs $\ln(Re)$

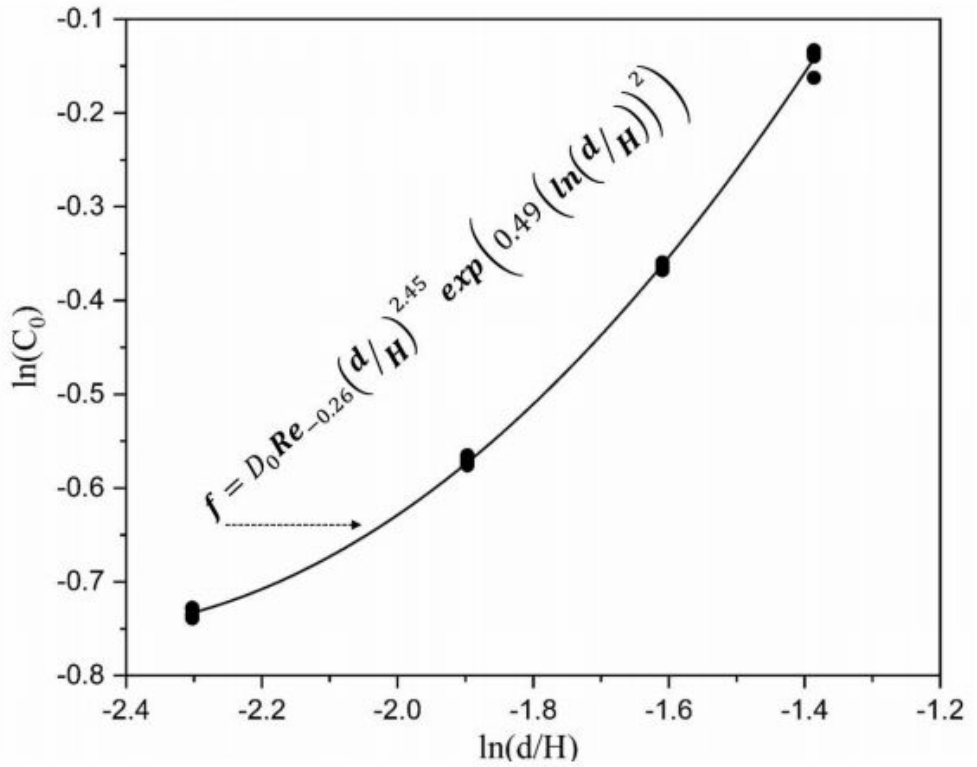

Figure 4.16: A plot of $\ln(C_0)$ vs $\ln(d/H)$

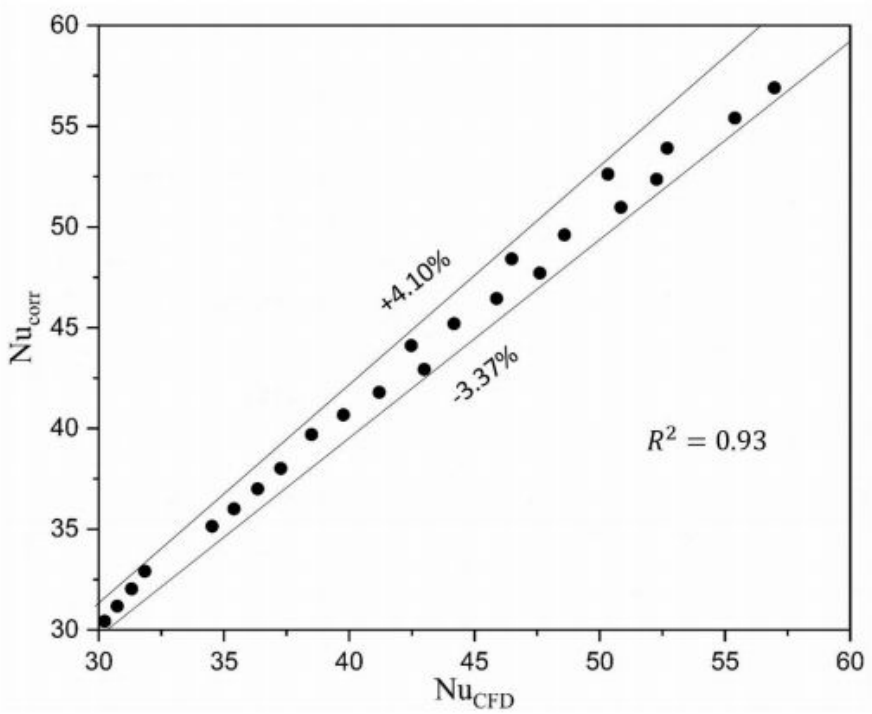

Figure 4.17: Comparison of predicted vs numerical values of Nusselt number

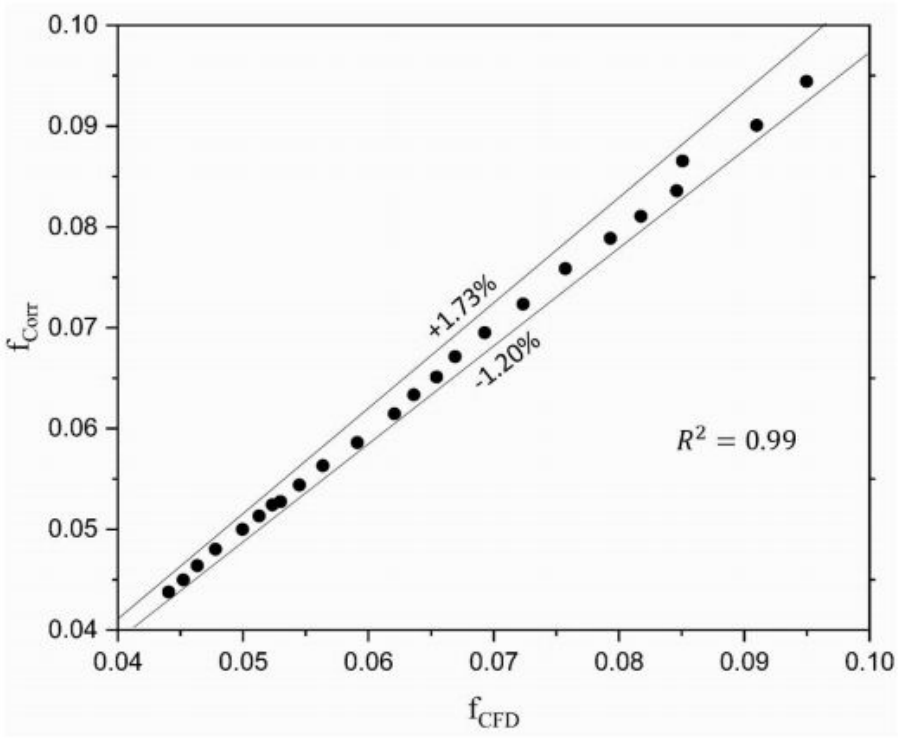

Figure 4.18: Comparison of predicted and numerical values of friction factor

4.5 Conclusions

A new design of a counter curved DPSAH was investigated and its thermohydraulic performance was compared with designs of parallel curved DPSAH under various flow and geometric parameters. The results show that with suitable heat transfer enhancement strategies such as curvature design passes, arrangement of fluid flow with strategically placed turbulators can play a significant role in overall performance improvement. Based on the results, main conclusions are given as follows:

- In curved design SAHs, counter DPSAH show better thermal performance than parallel DPSAH and smooth SPSAH. This is due to the counter-flow design having higher turbulence, longer duct length, and minimum top losses than other investigated SAHs. A counter design with curved double pass SAH shows almost double thermal efficiency than curved SPSAH

- The maximum increase of about 37 in thermal effectiveness was observed in roughened curved counter over parallel flow designs at Re and d/H values of 10000 and 0.25, respectively at $P/H = 0.75$.

- Rounded asymmetrically placed ribs reduces the system losses. The value of friction factor in descending order were observed as: roughened counter curved DPSAH > roughened parallel curved DPSAH > smooth counter curved DPSAH > smooth parallel curved DPSAH > smooth curved SPSAH.

- Based on the performance data, two new correlations of Nu and f were developed in terms of flow parameter (Re) and non-dimensional geometric ratio d/H. The correlation has the form: $Nu = k_1 Re^a (d/H)^b exp\left(k_2 \left(ln (d/H)^2\right)\right)$where k_1, k_2,a and$b$ are constants. A similar form was observed in friction factor variation with a negative exponent value of the constant a. The predicted Nu and$f$ from the established correlations match reasonably well with the data with a maximum deviation of 1.8 and 0.52, respectively.